Accurate Numerical Methods for Micromagnetics Simulations with General Geometries

Carlos J. García-Cervera∗, Zydrunas Gimbutas†, and Weinan E‡
∗ *Department of Mathematics, University of California, Santa Barbara, CA 93106. E-mail:* cgarcia@math.ucsb.edu. *URL:* http://www.math.ucsb.edu/~cgarcia
† *Department of Compute Science, Yale University, New Haven, CT 06520. E-mail:* zydrunas.gimbutas@yale.edu.
‡ *Department of Mathematics and Program in Applied and Computational Mathematics, Princeton University, Princeton, NJ 08544. E-mail:* weinan@princeton.edu. *URL:* http://www.math.princeton.edu/~weinan

Version: August 10, 2002

In current FFT-based algorithms for micromagnetics simulations the boundary is typically replaced by a staircase approximation along the grid lines, either eliminating the incomplete cells or replacing them by complete cells. Sometimes the magnetizations at the boundary cells are weighted by the volume of the sample in the corresponding cell. We show that this leads to large errors in the computed exchange and stray fields. One consequence of this is that the predicted switching mechanism depends sensitively on the orientation of the numerical grid. We present a boundary-corrected algorithm to efficiently and accurately handle the incomplete cells at the boundary. We show that this boundary-corrected algorithm greatly improves the accuracy in micromagnetics simulations. We demonstrate by using A. Arrott's example of a hexagonal element that the switching mechanism is predicted independently of the grid orientation.

Keywords

Micromagnetics, Landau-Lifshitz equation, stray field, Neumann problems, cartesian grid.

1. INTRODUCTION

Micromagnetic modeling of a ferromagnetic material has been an active area of research in the past decade, and is receiving even more attention because of the general interest in nano-scale physics [11]. Traditionally, interest in understanding the detailed magnetic domains and switching mechanisms has come from the magnetic recording industry. More recently, the program in designing magnetic random access memory (MRAM) devices has also given a significant push on the study of nano-scale defect structures in submicron elements [19, 6].

The dynamics of the magnetization distribution in a ferromagnetic material is described by the Landau-Lifshitz equation [12, 14]:

$$\frac{\partial \mathbf{M}}{\partial t} = -\gamma(\mathbf{M} \times \mathcal{H}) - \frac{\alpha\gamma}{M_s}\mathbf{M} \times (\mathbf{M} \times \mathcal{H}), \tag{1}$$

with the boundary condition

$$\frac{\partial \mathbf{M}}{\partial \nu} = 0 \tag{2}$$

where the vector ν represents the unit outward normal on the boundary of the ferromagnetic sample. In (1), $|\mathbf{M}| = M_s$ is the saturation magnetization, and is usually set to be a constant far from the Curie temperature; γ is the gyromagnetic ratio. The first term on the right hand side is the gyromagnetic term and the second term is the damping term. α is the dimensionless damping coefficient. $\mathcal{H}$ is the local field, computed from the Landau-Lifshitz free energy functional:

$$F(\mathbf{M}) = \frac{1}{2}\int_V \left\{ \frac{A}{M_s^2}|\nabla \mathbf{M}|^2 + \Phi\left(\frac{\mathbf{M}}{M_s}\right) - 2\mu_0 \mathbf{H}_e \cdot \mathbf{M} + \mu_0 \mathbf{M} \cdot \nabla U \right\} dx, \tag{3}$$

$$\mathcal{H} = -\frac{\delta F}{\delta \mathbf{M}} = \frac{A}{M_s^2}\Delta \mathbf{M} - \frac{1}{M_s}\Phi'\left(\frac{\mathbf{M}}{M_s}\right) + \mu_0 \mathbf{H}_e - \mu_0 \nabla U \tag{4}$$

In (3) and (4), A is the exchange constant, $A|\nabla \mathbf{M}|^2/M_s^2$ is the exchange interaction energy between the spins, $\Phi\left(\mathbf{M}/M_s\right)$ is the energy due to material anisotropy, μ_0 is the permeability of vacuum, $-2\mu_0 \mathbf{H}\cdot\mathbf{M}$ is the energy due to the external field, V is the volume occupied by the material, and finally the last term in (3) is the energy due to the field induced by the magnetization distribution inside the material. This induced field $\mathbf{H_s} = -\nabla \mathbf{U}$, or stray field, can be computed by solving the differential equation

$$\begin{aligned} \Delta U &= \nabla \cdot \mathbf{M}, \quad \text{in } V, \\ \Delta U &= 0, \quad \text{outside } V \\ [U] &= 0, \quad \text{across } \partial V \\ \left[\frac{\partial U}{\partial \nu}\right] &= -\mathbf{M} \cdot \nu, \quad \text{across } \partial V. \end{aligned} \tag{5}$$

Here we use [ ] to denote the jump of a quantity across the boundary of V, ∂V.

Equation (5) can be solved explicitly, and the solution is [21]

$$\begin{aligned} U(x) &= \nabla N * \mathbf{M} = \int_{\mathbb{R}^3} \nabla N(x-y) \cdot \mathbf{M}(y)\, dy \\ \mathbf{H_s} &= -\nabla U(x) = -\nabla \int_{\mathbb{R}^3} \nabla N(x-y) \cdot \mathbf{M}(y)\, dy \end{aligned} \tag{6}$$

where $N(x) = -\frac{1}{4\pi}\frac{1}{|x|}$ is the Newtonian potential in $\mathbb{R}^3$.

The main purpose of this paper is to provide an accurate way of evaluating the exchange and stray fields using FFT-based methods for more general geometries. We achieve this by carefully evaluating the contributions from the non-rectangular cells that appear near the boundary of the domain when a sample of arbitrary shape is discretized using a uniform grid. As an illustration of our method, we will investigate the sensitivity of the numerical results to grid orientation.

2. REVIEW OF NUMERICAL METHODS FOR MICROMAGNETICS SIMULATIONS

The basic idea commonly used in micromagnetics simulations is to decompose the domain into computational cells and approximate both the magnetization and the stray field, on each cell, by a constant representing its average value. The effective field is evaluated on each cell, and the magnetization is advanced in time using an appropriate time stepping scheme. Explicit schemes, such as fourth order Runge-Kutta, or predictor-corrector schemes, are most commonly used. Recently, a new unconditionally stable numerical time stepping procedure was presented in [25].

In broad terms, the numerical methods currently used for the simulation of the Landau-Lifshitz equation can be divided into two categories, according to how the nonlocal stray field is evaluated. The first class of methods solve approximately the differential equation (5) using an appropriate discretization, such as finite differences or finite elements. The difficulty with this approach is the lack of an effective boundary condition for U. The differential equation (5) is formulated in the entire space, which has to be truncated in simulations. Often a boundary integral equation is used to represent the correct boundary condition at ∂V [13, 3, 24].

The second class of methods is based on using (6) to compute the stray field. The convolution integral in (6) is replaced by some numerical quadrature, and the summation is performed, often by using the Fast Fourier Transform (FFT) [26, 10, 20, 4, 9]. As such, the underlying numerical grid should be uniform in order to be able to use FFT. Such an approach is quite successful when the material has a rectangular shape. Otherwise, as we demonstrate in this paper, it suffers from serious inaccuracies when the boundary ∂V cuts through numerical cells.

In order to compute the effective field, let us concentrate in the two dimensional situation.

Assume that the computational domain Ω is a rectangle with sides aligned with the coordinate axes which is subdivided into $m \times n$ rectangles Ω_{ij} and that both the magnetization and the stray field are represented by piecewise constant functions. Let $\mathbf{M}_{ij}$ and $\mathbf{H}_{ij}$ represent the value of the magnetization and the stray field inside each rectangle of the subdivision. We will approximate the stray field $\mathbf{H}$ inside Ω_{ij} by its mean value. Substituting $\mathbf{M}$ in (6) and averaging

$$\mathbf{H}_{ij} = -\sum_{kl} \frac{1}{|\Omega_{ij}|} \int_{\Omega_{ij}} \left(\nabla \int_{\Omega_{kl}} \nabla N(x-y)\, dy \right) dx \cdot \mathbf{M}_{kl} \tag{7}$$

Here we used the notation $|\Omega_{ij}| = \text{area}(\Omega_{ij})$. We define the mutual demagnetizing tensor for domains Ω_{ij} and Ω_{kl} as

$$D_{ijkl} = \frac{1}{|\Omega_{ij}|} \int_{\Omega_{ij}} \left(\nabla \int_{\Omega_{kl}} \nabla N(x-y)\, dy \right) dx \tag{8}$$

After integration by parts:

$$D_{ijkl} = -\frac{1}{|\Omega_{ij}|}\int_{\partial\Omega_{ij}}\left(\int_{\partial\Omega_{kl}} N(x-y)\nu_{kl}(y)\,d\sigma_{kl}(y)\right)\otimes\nu_{ij}(x)\,d\sigma_{ij}(x) \qquad (9)$$

where the vectors ν_{ij} and ν_{kl} are the unit outward normals on the boundary of Ω_{ij} and Ω_{kl} respectively. The tensor product of vectors $\mathbf{u}$ and $\mathbf{v}$, denoted by $\mathbf{u}\otimes\mathbf{v}$, is defined as the matrix with elements $(\mathbf{u}\otimes\mathbf{v})_{ij} = u_i v_j$.

It is easy to see that if the grid is uniform, the value of the demagnetizing tensor depends only on the differences $i-j$ and $k-l$, i.e., the tensor is translation invariant. Therefore the sum in (7) is a discrete convolution and can be efficiently computed by using the Fast Fourier Transform (FFT).

Computing the demagnetizing tensors is not a trivial task. Integrals in (9) are singular and difficult to evaluate either analytically or numerically. For rectangular cells, the analytic expression for the demagnetizing tensors have been obtained by Aharoni [1]. Somewhat more involved analytic expressions for the mutual demagnetizing tensors for arbitrary non-intersecting rectangular prisms aligned with the coordinate planes are given in [17].

In many applications the material is a thin film, and in this situation the evaluation of the demagnetizing tensor can be simplified. Assume that the volume V occupied by the material is $\Omega\times[-\delta,\delta]$, where Ω is a domain in the xy-plane and 2δ is the thickness of the film. If the thickness δ is small in comparison to the size of Ω, we can safely assume that the magnetization $\mathbf{M}$ is constant in the transversal direction to the film, and depends only on the in-plane coordinates. Under these assumptions, the effective stray field is given by

$$\mathbf{H}_s(x) = -\nabla\int_\Omega \nabla K_\delta(x-y)\cdot\mathbf{M}'(y)\,dy + \int_\Omega W_\delta(x-y)\cdot M_3(y)\,dy\cdot\mathbf{e}_3 \qquad (10)$$

where $\mathbf{M}'(x) = (M_1(x), M_2(x)) = M_1(x)\cdot\mathbf{e}_1 + M_2(x)\cdot\mathbf{e}_2$ are the in-plane components of the magnetization vector $\mathbf{M}(x) = (M_1(x), M_2(x), M_3(x))$, and $K_\delta : \mathbb{R}^2\to\mathbb{R}$ and $W_\delta : \mathbb{R}^2\to\mathbb{R}$ are defined by the formulas (see [8], for example),

$$K_\delta(x) = \frac{1}{2\pi}\operatorname{arcsinh}\left(\frac{2\delta}{|x|}\right) - \frac{1}{4\pi\delta}\left(\sqrt{|x|^2+4\delta^2} - |x|\right), \qquad (11)$$

where $\operatorname{arcsinh}(x) = \ln\left(x+\sqrt{x^2+1}\right)$ and

$$W_\delta(x) = \frac{1}{4\pi\delta}\left(\frac{1}{|x|} - \frac{1}{\sqrt{|x|^2+4\delta^2}}\right), \qquad (12)$$

respectively. Here we use the notation $\mathbf{e}_1 = (1,0,0), \mathbf{e}_2 = (0,1,0), \mathbf{e}_3 = (0,0,1)$. Consequently, the mutual demagnetizing tensor for domains Ω_{ij} and Ω_{kl} is given by

$$\mathbf{D}_{ijkl} = \begin{pmatrix} \overline{\mathbf{D}}_{ijkl} & 0 \\ 0 & D^{33}_{ijkl} \end{pmatrix}, \overline{\mathbf{D}}_{ijkl} = \begin{pmatrix} D^{11}_{ijkl} & D^{12}_{ijkl} \\ D^{21}_{ijkl} & D^{33}_{ijkl} \end{pmatrix}, \qquad (13)$$

where

$$\overline{\mathbf{D}}_{ijkl} = \frac{1}{|\Omega_{ij}|}\int_{\partial\Omega_{ij}}\left(\int_{\partial\Omega_{kl}} K_\delta(x-y)\cdot\nu_{kl}(y)\,d\sigma_{kl}(y)\right)\otimes\nu_{ij}(x)\,d\sigma_{ij}(x), \qquad (14)$$

and

$$D^{33}_{ijkl} = \frac{1}{|\Omega_{ij}|} \int_{\Omega_{ij}} \left(\int_{\Omega_{kl}} W_\delta(x-y)\, dx \right) dy, \tag{15}$$

The integrals in (14) are one dimensional and have logarithmic singularities. Furthermore, even if Ω_{ij} or Ω_{kl} have sharp corners, or some parts of their boundaries intersect or coincide, the gradient of the inner integral in (14)

$$\int_{\partial\Omega_{ij}} K_\delta(x-y) \cdot \nu_{ij}(y)\, d\sigma_{ij}(y) \tag{16}$$

is infinite at only a finite number of points and the adaptive numerical integration for the outer integral does not experience any difficulties. Finally, the computation of (15) can be avoided by using the trace property of the demagnetizing tensors

$$D^{33}_{ijkl} = \delta_{ik}\delta_{jl} - D^{11}_{ijkl} - D^{22}_{ijkl} \tag{17}$$

which derives from the fact that the Laplacian of the Newtonian potential is a Dirac distribution.

2.1. Staircase approximation

In current micromagnetics simulations of ferromagnetic materials of non-rectangular shape, it is customary to consider a rectangular computational domain that contains the ferromagnetic sample. The magnetization is set equal to zero outside the material and the rectangular domain is discretized using a uniform grid. This results in the appearance of cells of non-rectangular shape near the boundary of the material, as illustrated in Figure 1. It is a common practice to replace the boundary of the sample by a staircase, as in Figure 2. This has a dramatic effect on the accuracy of the results.

In order to illustrate this, we consider the example of a hexagonal permalloy element, suggested by A. Arrott [2]. This is also a good example to check the sensitivity of the numerically computed switching mechanism to grid orientation, since it is not possible to align the element with the coordinate axes. The long axis of the element is $1\mu m$, the width is $0.25\mu m$, and the thickness is $0.02\mu m$. The element was embedded into the computational domain with dimensions $1\mu m \times 1\mu m \times 0.02\mu m$. The initial magnetization was set to be parallel to the long axis, and then a gradually increased external field was applied in the opposite direction in order to simulate the reversal process. The external field was increased in increments of 2000 A/m and was kept constant at each field step until the steady state was reached. The Landau-Lifshitz equation was integrated using the standard 4th order Runge-Kutta method. The damping parameter α was set equal to 0.1. The physical constants were chosen to mimic permalloy ($M_s = 8.0 \times 10^5\ A/m$, $K_u = 5.0 \times 10^2\ J/m^3$, $A = 1.3 \times 10^{-11}\ J/m$, $\gamma = 1.76 \times 10^{11}\ T^{-1}s^{-1}$).

In Figure 3 we present images at different stages during the reversal process in the hexagonal sample, where the boundary has been approximated using the staircase approximation. We used 200 grid points in each direction to produce these results. In the first column we show the switching process for a sample at 0 degrees with respect to the OX axis. In the second column the sample has been rotated by 45 degrees in order to mimic the effect of a rotation of the numerical grid. Proper geometric scaling factors have been considered in order to make both simulations equivalent. The sequence shows two completely different switching mechanisms. In

both situations we observe initially the end domains grow, and the center domain shrinks. The results on the first column show that the switching occurs as a result of a rotation of the magnetization in the center domain, which subsequently spreads to the whole sample. The results on the second column, however, do not show such a rotation. What we see is the formation of vortices on the boundary of the sample. These vortices enter the sample and the orientation of the magnetization is reversed. The sequence also shows that, at 0 degrees, after the rotation of the magnetization in the interior of the sample has occurred, a series of vortices are generated on the boundary, and these vortices enter the sample, accelerating the reversal process.

Our experience and the experience of A. Arrott is that such spurious numerically produced switching does not disappear when the number of grid points in each direction is doubled.

This discrepancy in the switching mechanism is a result of the large errors introduced in the exchange and stray fields near the boundary of the material as a consequence of the staircase approximation. We present now corrections to the exchange and stray field that improve the results considerably.

3. BOUNDARY-CORRECTED METHOD

3.1. Corrections in the Exchange Field

The formation of vortices on the domain walls at the boundary, as seen in Figure 3.(h), is an indication that the exchange field is not being computed accurately near the boundary of the domain during the simulation. It is clear that the boundary condition (2) cannot be satisfied accurately using a staircase approximation since in such a case the numerical boundary of the material does not coincide with the prescribed physical boundary. This is the main source of errors in the exchange field.

One might argue that in reality the boundary of the sample is never accurately known and may contain rough edges. Nevertheless, it is important, as the subject matures, to be able to compute accurately the correct magnetization distribution once the boundary of the sample is given.

In the simulations presented in Figure 3 the exchange field was approximated using the standard five point formula for the laplacian

$$\Delta \mathbf{M}_{ij} \approx \frac{\mathbf{M}_{i+1,j} - 2\mathbf{M}_{i,j} + \mathbf{M}_{i-1,j}}{\Delta x^2} + \frac{\mathbf{M}_{i,j+1} - 2\mathbf{M}_{i,j} + \mathbf{M}_{i,j-1}}{\Delta y^2} \qquad (18)$$

where Δx and Δy are the grid sizes in the OX and OY directions respectively. To accurately evaluate the exchange field on the boundary cells, the value of $\mathbf{M}$ at exterior cells must be modified in order to take into account the boundary condition (2). Here we describe a general procedure to produce a second order accurate approximation to the laplacian on the cells near the boundary, taking into account the boundary condition (2).

To illustrate the procedure, we will consider first the one dimensional case. Consider the situation described in Figure 4. The points x_0, x_1, and x_2 are inside the domain, and the vales f_0, f_1, and f_2 are known. The point x_3 is outside the domain, and the value f_3 is to be determined. We want to approximate the second derivative of the function $f(x)$ at x_2, knowing that $f'(x_2 + \alpha\Delta x) = 0$. We consider

the fourth order accurate interpolation polynomial

$$p(x) = f_0 + \frac{f_1 - f_0}{\Delta x}(x - x_0) + \frac{f_2 - 2f_1 + f_0}{2\Delta x^2}(x - x_0)(x - x_1) + \frac{f_3 - 3f_2 + 3f_1 - f_0}{6\Delta x^3}(x - x_0)(x - x_1)(x - x_2) \quad (19)$$

We impose the boundary condition:

$$0 = p'(x_2 + \alpha\Delta x) = \frac{f_1 - f_0}{\Delta x} + \frac{f_2 - 2f_1 + f_0}{2\Delta x^2}(3 + 2\alpha)\Delta x + \frac{f_3 - 3f_2 + 3f_1 - f_0}{6\Delta x^3}(2 + 6\alpha + 3\alpha^2)\Delta x^2 \quad (20)$$

Thus we obtain:

$$f_3 \;=\; 3f_2 - 3f_1 + f_0 - \frac{6}{2 + 6\alpha + 3\alpha^2}\left(f_1 - f_0 + \frac{f_2 - 2f_1 + f_0}{2}(3 + 2\alpha)\right) \quad (21)$$

We approximate the second derivative at x_2 by:

$$f_2'' \approx p''(x_2) = \frac{f_3 - 2f_2 + f_1}{\Delta x^2} \quad (22)$$

Approximation (22) is second order accurate. The details of the proof can be obtained from the authors upon request. Note also that the coefficients in expression (22) can be bounded independently of α, and therefore the stability of the time-stepping scheme is not affected.

In the general case, we proceed in the same fashion. We think of the function $\mathbf{M}$ as a smooth function defined on Ω, and the value $\mathbf{M}_{ij}$ as the value of $\mathbf{M}$ at the center of the computational cell Ω_{ij}. Consider now a situation like the one depicted in Figure 5. We want to evaluate the laplacian on the cell (i, j) to high order accuracy. In order to do this, we define a fourth order accurate interpolation polynomial using all the points labeled in the picture (except $\mathbf{M}_{i+\beta,j-\frac{1}{2}}$ and $\mathbf{M}_{i+\frac{1}{2},j+\alpha}$, which are not grid points). Note that in two dimensions we need ten nodes to define such a polynomial:

$$\begin{aligned} p(x,y) = {} & \mathbf{a}_0 + \mathbf{a}_1(x - x_i) + \mathbf{a}_2(y - y_j) + \mathbf{a}_3(x - x_i)(x - x_{i-1}) + \mathbf{a}_4(y - y_j)(y - y_{j-1}) \\ & + \mathbf{a}_5(x - x_i)(y - y_j) + \mathbf{a}_6(x - x_i)(x - x_{i-1})(x - x_{i-2}) + \mathbf{a}_7(x - x_i)(x - x_{i-1})(y - y_j) \\ & + \mathbf{a}_8(x - x_i)(y - y_j)(y - y_{j-1}) + \mathbf{a}_9(y - y_j)(y - y_{j-1})(y - y_{j-2}) \end{aligned} \quad (23)$$

where the coefficients $\mathbf{a}_1, \mathbf{a}_2, \ldots, \mathbf{a}_9$ are determined by using the interpolatory conditions.

We impose the boundary conditions

$$\begin{aligned} \frac{\partial p}{\partial \nu}(x_i + \beta\Delta x, y_j - \frac{1}{2}\Delta y) &= 0 \\ \frac{\partial p}{\partial \nu}(x_i - \frac{1}{2}\Delta x, y_j + \alpha\Delta y) &= 0 \end{aligned} \quad (24)$$

Let us denote by $\nu^\alpha = (\nu_1^\alpha, \nu_2^\alpha)$ and $\nu^\beta = (\nu_1^\beta, \nu_2^\beta)$ the unit outward normal at the points $(x_i - \frac{1}{2}\Delta x, y_j + \alpha\Delta y)$ and $(x_i + \beta\Delta x, y_j - \frac{1}{2}\Delta y)$, respectively. Then equations

(24) become

$$\begin{aligned}
\frac{\partial p}{\partial x}(x_i + \beta\Delta x, y_j - \frac{1}{2}\Delta y)\nu_1^\beta + \frac{\partial p}{\partial y}(x_i + \beta\Delta x, y_j - \frac{1}{2}\Delta y)\nu_2^\beta &= 0 \\
\frac{\partial p}{\partial x}(x_i - \frac{1}{2}\Delta x, y_j + \alpha\Delta y)\nu_1^\alpha + \frac{\partial p}{\partial y}(x_i - \frac{1}{2}\Delta x, y_j + \alpha\Delta y)\nu_2^\alpha &= 0 \qquad (25)
\end{aligned}$$

This is a 2×2 system of equation with two unknowns, $\mathbf{M}_{i+1,j}$ and $\mathbf{M}_{i,j+1}$, which can be easily solved. The laplacian at (i, j) can be approximated by

$$\Delta\mathbf{M}_{i,j} \approx \Delta p(x_i, y_j) = \frac{\mathbf{M}_{i+1,j} - 2\mathbf{M}_{i,j} + \mathbf{M}_{i-1,j}}{\Delta x^2} + \frac{\mathbf{M}_{i,j+1} - 2\mathbf{M}_{i,j} + \mathbf{M}_{i,j-1}}{\Delta y^2} \qquad (26)$$

One can show that approximation (26) is second order accurate. The details can be obtained from the authors upon request. To avoid stability problems, one can use an external point that is two grid-points away from the boundary, instead of just one grid point away. A similar technique has been used in the context of Immerse Boundary problems [16, 15, 7]. The advantage of our approach is that it is not necessary to perform a local change of variables around the boundary of the domain.

In the case of the hexagon considered previously, this simplifies greatly. First, observe that if a boundary of the sample coincides with a grid line, then we can still use formula (18) without modifications. This follows from the following observation: On a boundary like the one depicted in Figure 6 the assignment $\mathbf{M}_{i,j+1} = \mathbf{M}_{i,j}$ would give a second order accurate approximation to the laplacian at (i, j). However the torque $\mathbf{M}_{i,j} \times \Delta_h M_{i,j}$ at (i, j) would not be affected if we simply set $\mathbf{M}_{i,j+1} = 0$, since $\mathbf{M}_{i,j} \times \mathbf{M}_{i,j} = 0$.

On the boundaries that are not parallel to the coordinate axes we have a situation like the one depicted in Figure 7. In this case, we assign $\mathbf{M}_{i+1,j} = \mathbf{M}_{i,j-1}$, and $\mathbf{M}_{i,j+1} = \mathbf{M}_{i-1.j}$.

The results obtained with these corrections in the exchange field are presented in Figure 8. As before, in the first column we show the results of the simulation with the hexagon at 0 degrees with respect to the OX axis. In the second column the hexagon has been rotated by 45 degrees. The main observation is that now the first stage of the switching process, which corresponds with the rotation of the magnetization in the center of the sample, is common to both simulations: The spurious vortices seen in Figure 3.(h) have been eliminated. However, we observe that after the interior rotation has occurred, a series of vortices appear on the boundary, and proceed to the interior, much like in Figure 3.(e). The presence of these vortices is due mainly to the errors in the stray field.

3.2. Corrections in the Stray Field

In order to correct the errors in the stray field that result from using the staircase approximation, the geometric shape of the boundary cells must be taken into account, as illustrated in Figure 1.

The efficient and accurate evaluation of the stray field presents two additional difficulties now. First, the evaluation of the demagnetization factors becomes more complicated since we need to evaluate the interaction between cells of arbitrary

shape. Second, the standard FFT-based algorithm is no longer applicable, since the demagnetizing tensors are no longer translation invariant.

We solve the first problem using a combination of analytic formulas and numerical integration for the demagnetizing tensors. For arbitrary non-intersecting bodies we evaluate the integrals in (9) using adaptive numerical integration [22, 5, 23]. The problems arise if the two domains coincide or have an edge in common. While the inner integral in (9)

$$\int_{\partial\Omega_{kl}} N(x-y)\cdot\nu_{kl}(y)\,d\sigma_{kl}(y) \tag{27}$$

can be obtained accurately, the outer integral is much more difficult to handle by most numerical integration programs, due to the large gradients of (27) near the corners of Ω_{kl}. Special quadrature may be applied to accelerate the convergence [5]. For thin films we use formulas (13), (14), and (15), and adaptive Gaussian quadrature. In our numerical experiments we have been able to compute all integrals to double precision accuracy.

The loss of translation invariance due to the irregular cells near the boundary is more difficult to deal with. Our strategy is to express the stray field as the sum of two contributions: the field produced by distant cells, or far field, and the field produced by the near neighbors, or near field. A similar method is presented in [18].

$$\mathbf{H}_{ij} = \mathbf{H}_{ij}^{(near)} + \mathbf{H}_{ij}^{(far)}. \tag{28}$$

Each contribution is evaluated in a different way. The near field only involves nearest neighbors, as illustrated in Figure 9:

$$\mathbf{H}_{ij}^{(near)} = -\sum_{|k-i|\le 1,|j-l|\le 1} \mathbf{D}_{ijkl}\cdot\mathbf{M}_{kl} \tag{29}$$

Hence it can be computed by direct summation in $O(N)$ operations, where N is the number of grid points.

The evaluation of the far field is somewhat more complicated. Instead of evaluating it exactly, we approximate it: We substitute the boundary cells by rectangles, just like in the staircase approximation described earlier. The value of the magnetization in these modified cells is rescaled in such a way that the net magnetization remains unchanged. Since the main contribution to the far field from a distant cell is due to the net magnetization in that cell, we expect this to be a good approximation. The advantage of this procedure is that by using only rectangular cells, the demagnetizing tensor becomes translation invariant, and the summation can be performed using the FFT in $O(N\log_2 N)$ operations. Notice that this step is now the main source of the error. The near field, however, is computed exactly.

The results of the boundary-corrected algorithm are shown in Figure 10. The improvement in the results is clear. The interior rotation of the magnetization is followed by the formation of a boundary layer, which disappears once the interior domain walls are pushed to the boundary. This mechanism, captured in both simulations, coincides with the switching mechanism commonly observed in rectangular samples which display an S state configuration, described in Figure 11.

For comparison, we present in Figure 12 various hysteresis loops obtained with and without corrections. The dimensions of the sample were $1\mu m \times 1\mu m \times 200$Å. The hysteresis loop was calculated quasi statically. Starting from a value $H_e = 0$ T,

the applied field was decreased in steps of 0.002 T when equilibrium was reached. Two criteria were used to determine that a steady state had been reached: either the simulation had run for 10 nanoseconds, or the relative change in the average magnetization after 10 steps was less than 10^{-6}. We performed simulations at 0 degrees and at 45 degrees. The results at 45 degrees were computed with both the staircase approximation and the boundary corrected algorithm. No corrections were necessary for the sample at 0 degrees. The results for the boundary corrected algorithm for a 200×200 grid coincided with the results obtained with the sample at 0 degrees. Reducing the grid size produced the same hysteresis loop. The boundary corrected algorithm with a 100×100 grid produced the same results as the staircase approximation with a 200×200 grid, indicating the improvement achieved by adding the boundary corrections.

4. CONCLUSION

We have shown that the staircase approximation leads to very large errors in the computation of the exchange and stray fields. We have presented an efficient boundary-corrected algorithm that handles directly and accurately the incomplete cells at the boundary. Experiments with A. Arrott's example of a hexagonal element show that the boundary-corrected algorithm produces results that are insensitive to grid orientation.

5. ACKNOWLEDGMENTS

We thank A. Arrott for suggesting the example of a hexagonal element. We also thank R. Koch and J. Shi for helpful discussions. The first author thanks Hector Ceniceros for helpful discussions. The work of Z. Gimbutas and W. E was supported in part by NSF via a PECASE award.

REFERENCES

[1] A. Aharoni. Demagnetizing factors for rectangular ferromagnetic prisms. *J. Appl. Phys.*, 83:3432–3435, 1998.

[2] A. Arrot. private communication.

[3] D.V. Berkov, K. Ramstöck, and A. Hubert. Solving micromagnetic problems: Towards an optimal numerical method. *Phys. Stat. Sol. (a)*, 137:207–225, 1993.

[4] J.L. Blue and M.R. Scheinfein. Using multipoles decreases computation time for magnetic self-energy. *IEEE Trans. Magn.*, 27:4778–4780, 1991.

[5] H. Cheng, V. Rokhlin, and N. Yarvin. Nonlinear optimization, quadrature, and interpolation. *SIAM J. Optim.*, 9:901–923, 1999.

[6] J. Daughton. Magnetoresistive memory technology. *Thin Solid Films*, 216:162–168, 1992.

[7] Aaron L. Fogelson and James P. Keener. Immersed Interface Methods for Neumann and related problems in two and three dimensions. *SIAM J. Sci. Comput.*, 22:1630–1654, 1999.

[8] Carlos J. García-Cervera. *Magnetic Domains and Magnetic Domain Walls.* PhD thesis, Courant Institute of Mathematical Sciences, New York University, 1999.

[9] NIST MICROMAGNETIC MODELING ACTIVITY GROUP. http://www.ctcms.nist.gov/~rdm/mumag.html.

[10] N. Hayashi, K. Saito, and Y. Nakatani. Calculation of demagnetizing field distribution based on fast fourier transform of convolution. *Jpn. J. Appl. Phys.*, 35:6065–6073, 1996.

[11] National Nanotechnology Initiative. A report by Interagency Working Group on Nanoscience, Engineering, and Technology, Committee on Technology, National Science and Technology Council, Washington, D.C., 2000.

[12] W.F. Brown Jr. *Micromagnetics.* Interscience Tracts on Physics and Astronomy. Interscience Publishers (John Wiley and Sons), New York - London, 1963.

[13] T.R. Koehler and D.R. Fredkin. Finite element methods for micromagnetics. *IEEE Transactions on Magnetics*, 28:1239–1244, 1992.

[14] L. Landau and E. Lifshitz. On the theory of the dispersion of magnetic permeability in ferromagnetic bodies. *Physikalische Zeitschrift der Sowjetunion*, 8:153–169, 1935.

[15] Randall J. Leveque and Zhilin Li. The Immersed Interface Method for elliptic equations with discontinuous coefficients and singular sources. *SIAM J. Numer. Anal.*, 31:1019–1044, 1994.

[16] Zhilin Li. A fast iterative algorithm for elliptic interface problems. *SIAM J. Numer. Anal.*, 35:230–254, 1998.

[17] A.J. Newell, W. Williams, and D.J. Dunlop. A generalization of the demagnetizing tensor for nonuniform magnetization. *J. Geophysical Research*, 98:9551–9555, 1993.

[18] Joel R. Phillips and Jacob K. White. A Precorrected-FFT Method for Electrostatic Analysis of Complicated 3-D Structures. *IEEE Transactions on Computer-Aided Design of Integreated Circuits and Systems*, 16:1059–1072, 1997.

[19] G. Prinz. Magnetoelectronics. *Science*, 282:1660, 1998.

[20] T. Schrefl, J. Fidler, and H. Kronmüller. Nucleation fields of hard magnetic particles in 2d and 3D micromagnetic calculations. *J. Magn. Magn. Mat.*, 138:15–30, 1994.

[21] Albert Shadowitz. *The Electromagnetic Field.* Dover Publicacions, Inc., 1975.

[22] J. Strain. Locally corrected multidimensional quadrature rules for singular functions. *SIAM J. Scientific Comp.*, 16:992–1017, 1995.

[23] A. H. Stroud and D. Secrest. *Gaussian Quadrature Formulas.* Prentice-Hall, New York, 1966.

[24] Semyon V. Tsynkov. Numerical solution of problems on unbounded domains. A review. *Appl. Num. Math.*, 27:465–532, 1998.

[25] Xiao-Ping Wang, Carlos J. García Cervera, and Weinan E. A Gauss-Seidel Projection Method for the Landau-Lifshitz equation. *J. Comp. Phys.*, 171:357–372, 2001.

[26] Samuel W. Yuan and Neal Bertram. Fast adaptive algorithms for micromagnetics. *IEEE Transactions on Magnetics*, 28(5):2031–2036, 1992.

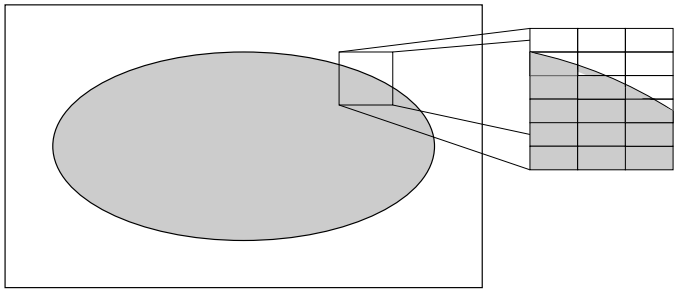

FIG. 1 Irregular cells near the boundary of the sample when a uniform discretization is used.

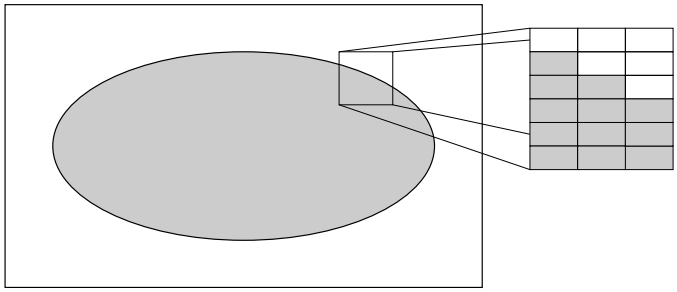

FIG. 2 Staircase approximation: The irregular cells near the boundary have been replaced by rectangles.

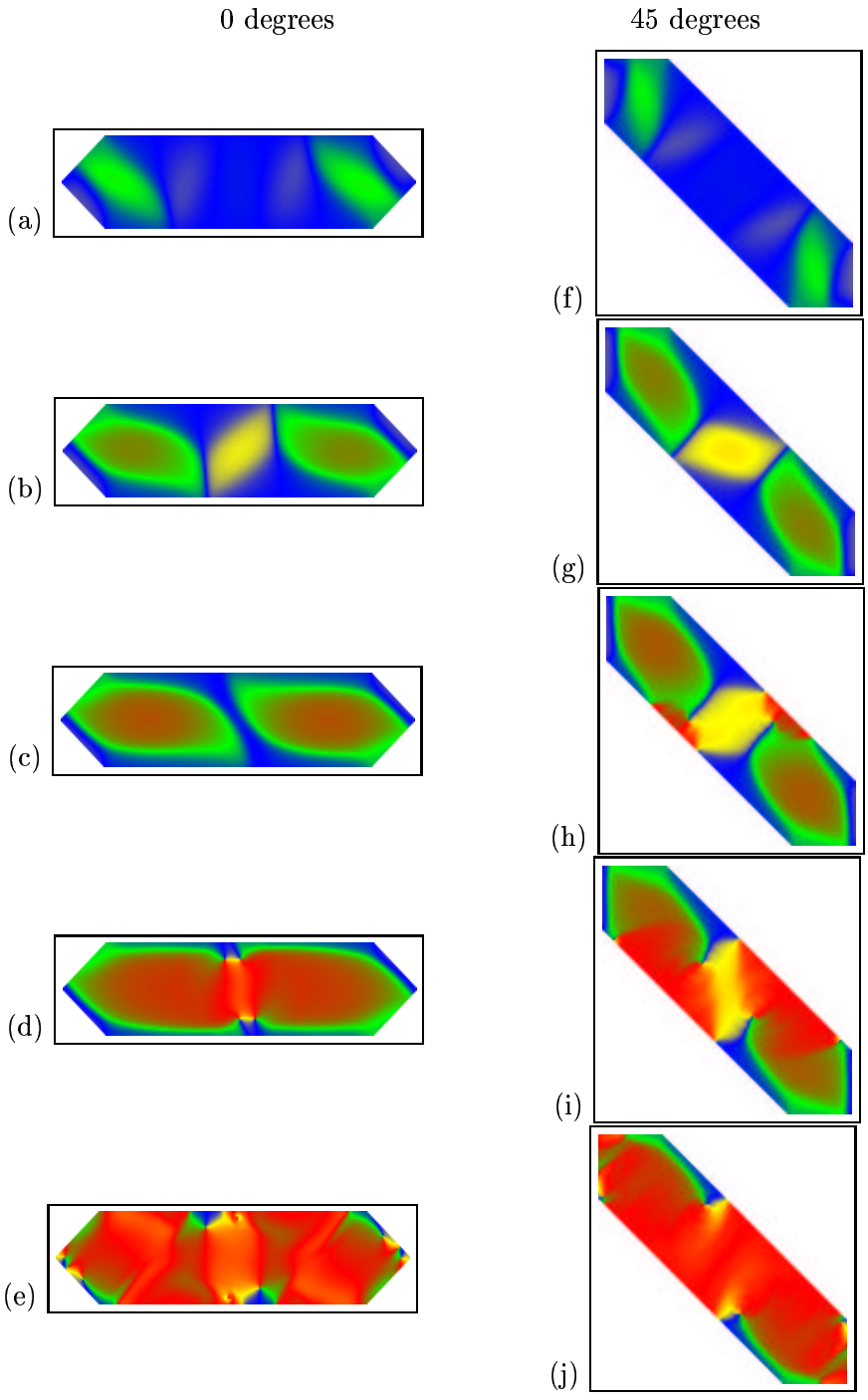

FIG. 3 Reversal in a hexagonal sample using the staircase approximation in both the exchange and the stray fields: (a)-(c) Enlargement of the end domains. (d) Interior Rotation. (e) Generation of vortices at the boundary. (f)-(g) Enlargement of the end domains. (h)-(j) Vortices appear on the boundary and enter the domain, causing the reversal of the magnetization.

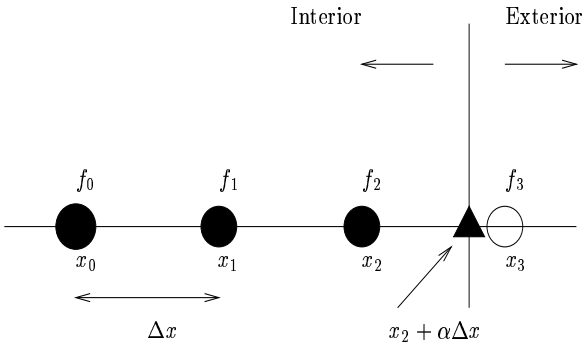

FIG. 4 High order approximation of the second derivative in the one dimensional case.

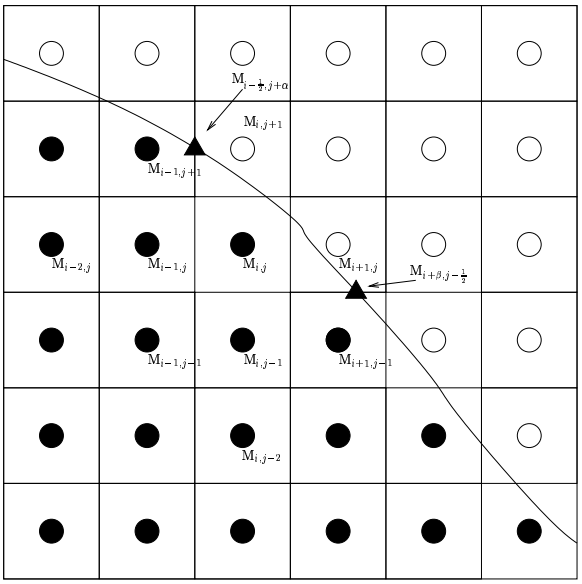

FIG. 5 Extended stencil near the boundary. Only the grid points used for the interpolation polynomial are labeled. We include the cases $\alpha = 0$ and $\beta = 0$, in which case a grid point is precisely on the boundary of the sample.

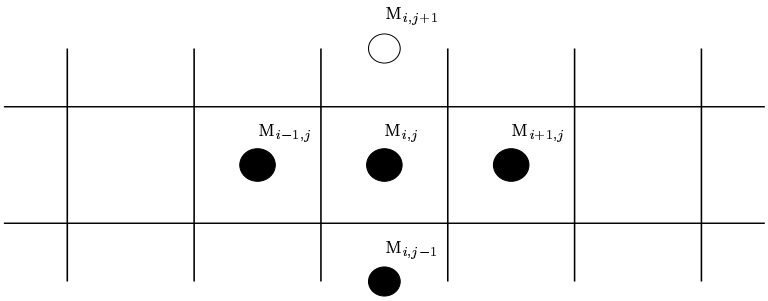

FIG. 6 The boundary coincides with one of the gridlines.

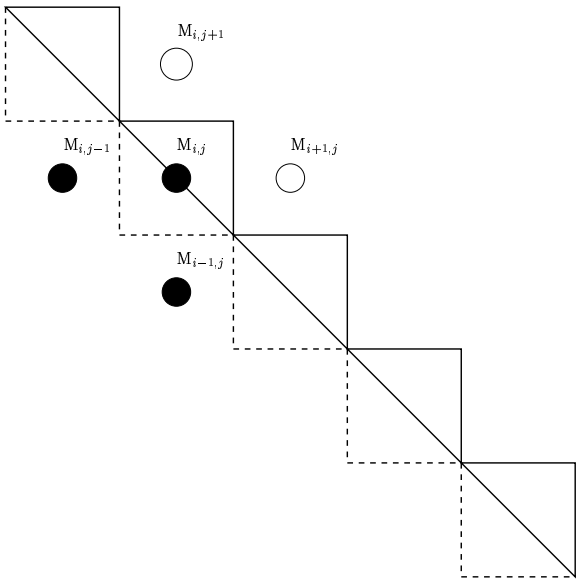

FIG. 7 Boundary of the hexagon. Both α and β are zero. We do not need to increase the stencil in this case.

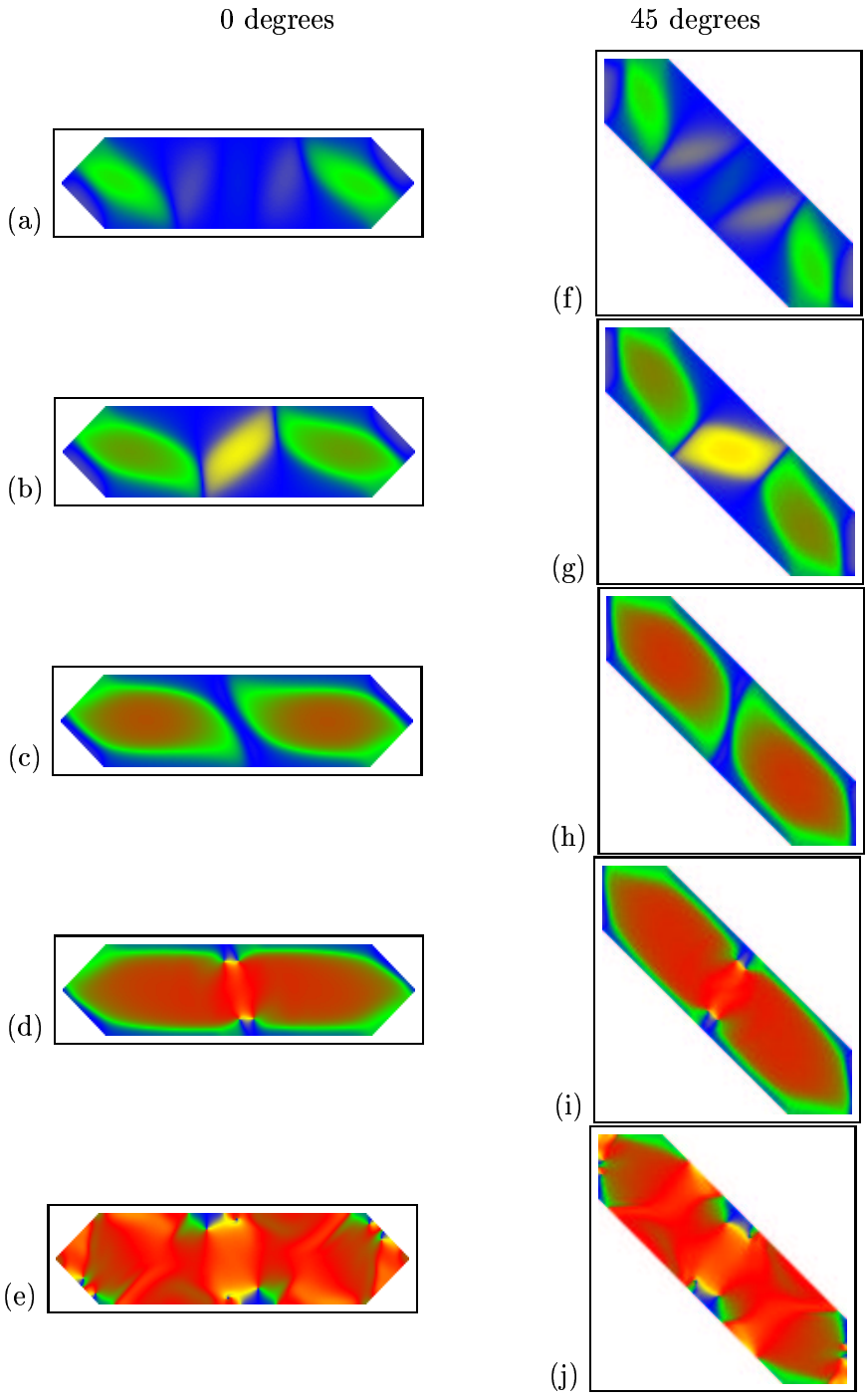

FIG. 8 Reversal in a hexagonal sample using the staircase approximation in the stray field. The exchange field is computed to second order accuracy everywhere. (a)-(d) and (f)-(i) show the growth of the end domains and the interior rotation of the magnetization. (e) and (j) show the subsequent formation of vortices on the boundary.

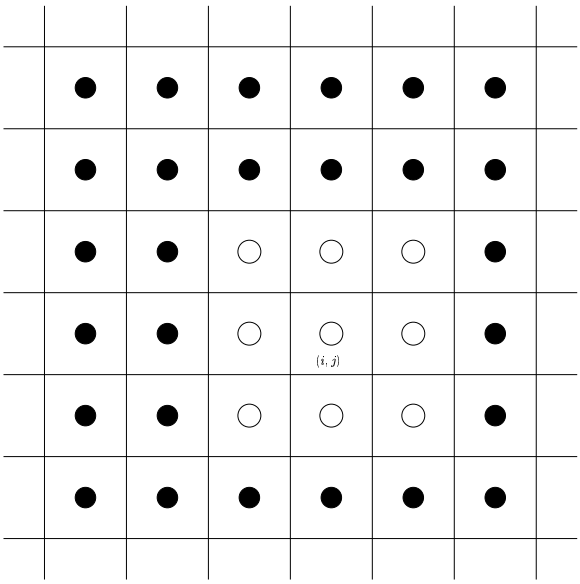

FIG. 9 Near field and Far field at cell (i, j). For the Near field, only the white cells are used. For the Far field, the black cells are used.

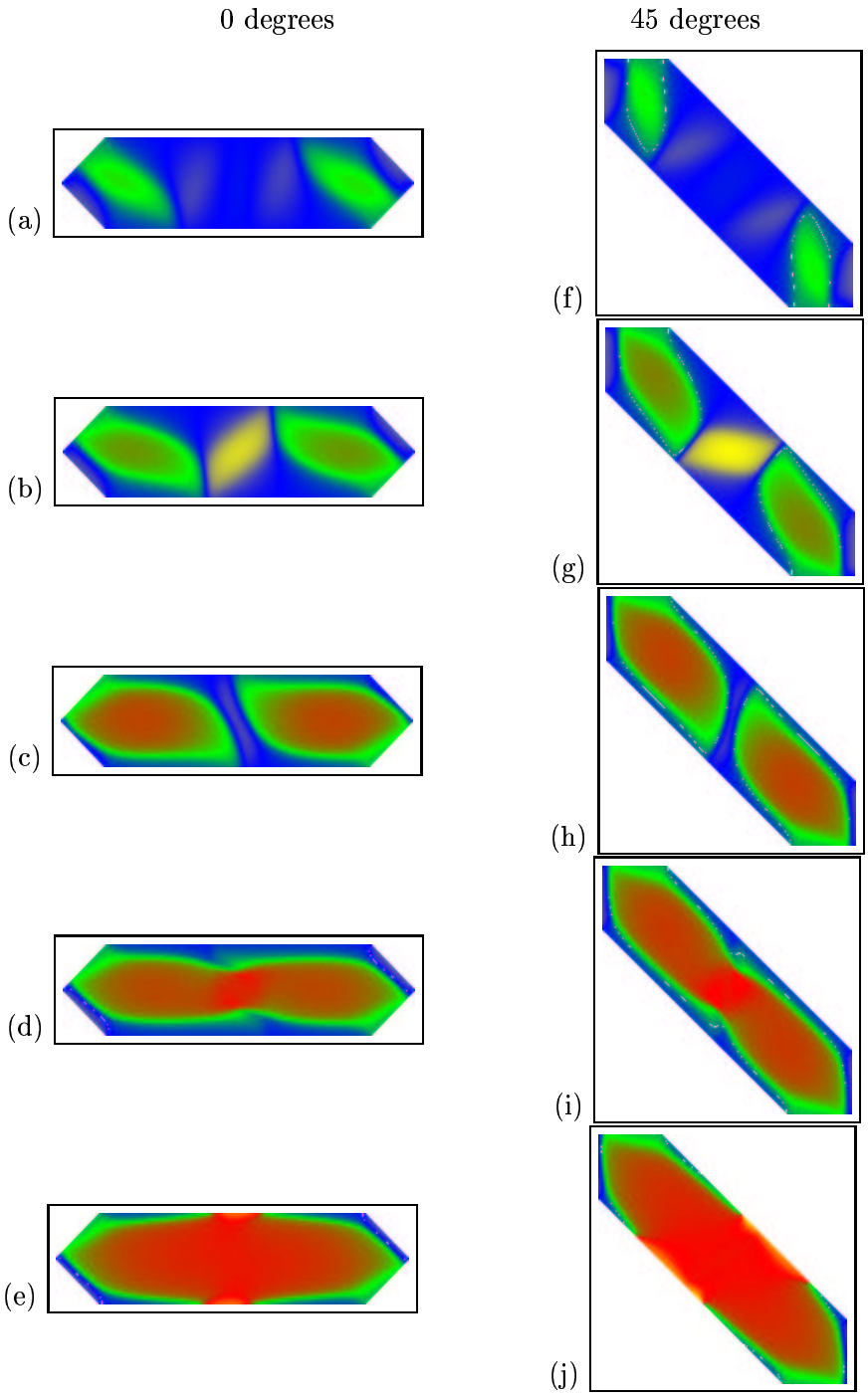

FIG. 10 Reversal in a hexagonal sample using the boundary-corrected algorithm. Corrections for the exchange and stray fields have been added. The results are insensitive to grid orientation. (a)-(d) and (f)-(i) show the growth of the end domains and the interior rotation of the magnetization. (e) and (j) show how the domain walls are pushed to the boundary. No vortices are present.

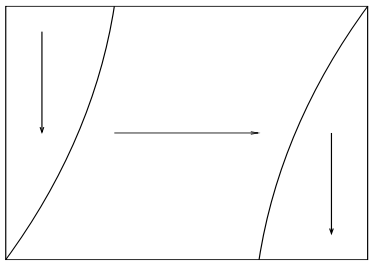

FIG. 11 Sketch of the magnetization distribution for an S state configuration in a rectangular cell.

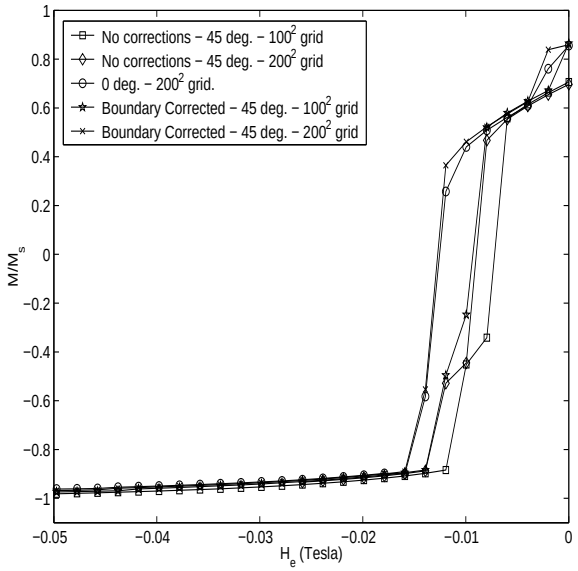

FIG. 12 Hysteresis loops computed with and without corrections, at 0 and 45 degrees.